

Loess deposits in southern Tajikistan (Central Asia): Magnetic properties and paleoclimate

Nazarov Parviz ^{a,c,d,e,*}, Zhongshan Shen ^{b,c}, Mamadjanov Yunus ^f, Sajid Zulqarnain ^a

^a Key Laboratory of Cenozoic Geology and Environment, Institute of Geology and Geophysics, Chinese Academy of Sciences, Beijing, 100029, China

^b State Key Laboratory of Lithospheric Evolution, Institute of Geology and Geophysics, Chinese Academy of Sciences, Beijing, 100049, China

^c College of Earth and Planetary Sciences, University of Chinese Academy of Sciences, Beijing, 100049, China

^d Innovation Academy for Earth Science, Chinese Academy of Sciences, Beijing, 100029, China

^e CAS Center for Excellence in Life and Paleoenvironment, Beijing, 100044, China

^f Institute of Geology, Earthquake Engineering and Seismology of the Academy of Sciences of the Republic of Tajikistan, Dushanbe, 734063, Tajikistan

ARTICLE INFO

Keywords:

Loess
Paleomagnetism
Pleistocene
Paleoclimate
Tajikistan
Central Asia

ABSTRACT

The continental accumulation of dust during the Quaternary led to the formation of widespread loess deposits in southern Tajikistan. In this area, the accumulation of loess is commonly associated with the occurrence of dust storms and the widespread distribution of loess provides evidence of dust storms becoming more frequent in arid Central Asia at least since the Early Pleistocene. Southern Tajikistan represents one of the largest loess deposits in Central Asia. We conducted a thorough study on the magnetostratigraphy, grain size, and magnetic susceptibility of the Chashmanigar section to reconstruct the stratigraphy of loess deposits and paleoclimate of Tajikistan. Based on our new data, the lower boundary of the basal ages of the Olduvai and Reunion subchrons were established for the studied Chashmanigar section. Rock magnetic analyses showed that the predominant ferrimagnetic minerals are large pseudo-single domain grains of magnetite, including limited maghemite. Standard demagnetization techniques yielded a characteristic component of natural remanent magnetization, which was used to obtain a well-defined magnetostratigraphy. In southern Tajikistan, paleosols consistently exhibit finer grain size distribution and higher magnetic susceptibility than loess horizons, suggesting that the environment of the Chashmanigar section was colder, drier, and dustier during glacial periods than during interglacial periods. Through correlation with astronomically tuned oxygen isotope records, sophisticated dating of the loess-paleosol sequence at Chashmanigar could be achieved, and the global significance of the recorded paleoclimatic variations could be revealed. The resulting grain size, magnetic susceptibility, and correlation with astronomically tuned oxygen isotope clearly provide information about the climatic pattern during the Early Pleistocene.

1. Introduction

Previous studies of loess-paleosol sequences have provided abundant information about regional and global climate evolution during the Quaternary period (Heller and Liu, 1985; Kukla, 1987; Ding et al., 1994; Porter and Zhisheng, 1995). The accumulation of loess in Central Asia has been receiving increasing attention from Quaternary researchers (Bronger et al., 1998; Shackleton et al., 1999; Ding et al., 2002b). The Central Asian piedmont loess provides near-continuous records of sedimentary accumulation in response to climatic change (Ding et al., 2002b), similar to the substantial deposits of the Chinese Loess Plateau. Thus, the study of the thick and continuous southern Tajikistan loess is

very important to link variations in the regional climate of Central Asia and the global climate. Several thousands of tons of dust have been transported by dust storms and accumulated in river valleys and on watershed plateaus in piedmont areas (Frechen and Dodonov, 1998a). As Central Asia lies far from oceanic sources of moisture, the climate in Central Asia is dominated by the westerlies and the subtropical high. The consequent insufficiency of water resources and sparse vegetation cover have led to a fragile ecosystem and sensitive climate (Jia et al., 2018). Through its contribution to the planetary albedo (Dirmeyer and Shukla, 1996) and through dust emissions, the ecosystem of a given region can influence the climate (Maher et al., 2010). In Tajikistan (Central Asia), moisture is derived directly or via recycling from the

* Corresponding author. Key Laboratory of Cenozoic Geology and Environment, Institute of Geology and Geophysics, Chinese Academy of Sciences, Beijing, 100029, China.

E-mail address: parviz_53@mail.ru (N. Parviz).

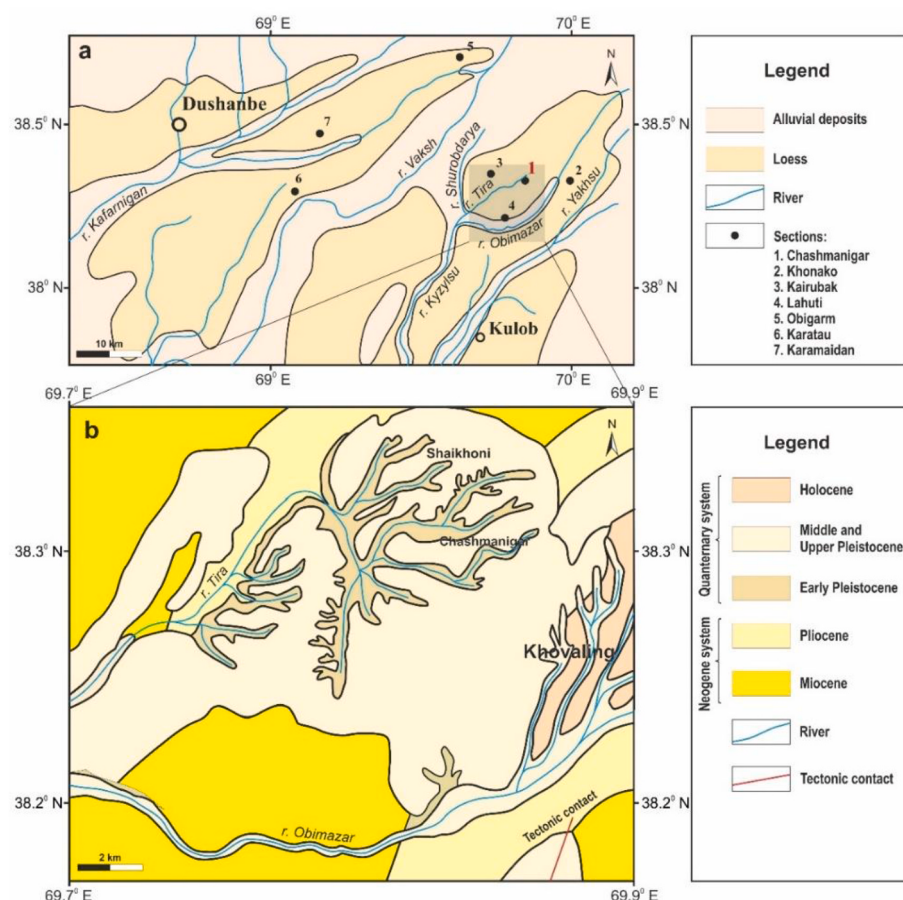


Fig. 1. a) Loess distribution and key sections in southern Tajikistan, modified after Dodonov and Baiguzina (1995). b) Geological map of southern Tajikistan modified after Philonov and Korol (1964).

Black and Caspian Seas, from the Mediterranean or North Atlantic (Aizen et al., 2006). Accordingly, it is important to understand the climatic evolution and mechanisms of climate change in Central Asia

(Chen et al., 2010, 2016; Leroy et al., 2013).

During the Quaternary period, accumulation of wind-blown dust led to the formation of a widespread and thick loess cover on piedmonts of



Fig. 2. Chashmanigar loess section in Khovaling, Tajikistan.

mountains in Tajikistan. The loess-paleosol formation of southern Tajikistan belongs to Pleistocene sediments, which unconformably overlie Neogene deposits. Hypsometrically, the upper limit of the distribution of loess is typically limited to 2000–2200 m. Above these absolute marks, loess is often absent or present in the form of low-power fragmentary covers, sometimes reaching absolute heights of up to 3000 m (Dodonov, A. E., 2007). Source materials of the loess in Tajikistan originate from the Tianshan mountains and western edge of the Pamir mountains. These materials were transported by rivers (Syr-Darya, Amu-Darya, Kyzylsu, Yakhshu, Vakhsh) to deflation sites, which consist of pluvial fans, floodplains, and the Karakum and Kyzylkum deserts from east to west, with the distribution direction being essentially parallel to the general direction of the rivers (Dodonov, 1991; Dodonov and Bajguzina, 1995). These deserts served as transfer stations of eolian dust for the loess region. All of these processes finally led to extensive and thick loess deposits in southern Tajikistan and therefore provide a unique opportunity to reconstruct the paleoclimate of Central Asia. Consequently, the thick layer of continuously deposited loess in southern Tajikistan is one of the most important archives of the paleoclimate in Central Asia.

The age of the upper part of the southern Tajikistan loess section was established by Frechen and Dodonov (1998a) using thermoluminescence (TL) and infrared stimulated luminescence (IRSL). Thereafter, Ding et al. (2002b) provided new paleomagnetic data and tentatively confirmed the beginning of the typical loess deposit (Chashmanigar section) to be during the Olduvai period. Unfortunately, the section was blocked by slope wash and provided the change of dust accumulation during the last 1.78 Ma and a total of 24 paleosols (S₁–S₂₄) have been

determined to be distinguishable above a depth of 195 m at Chashmanigar, which is dated around the top of the Olduvai subchron (Ding et al., 2002b). Accordingly, the onset of the natural exposure of the southern Tajikistan Chashmanigar loess section remains unclear, which hinders further investigation of the climatic pattern and the long-time/term scale of environmental change during the Early Pleistocene in Central Asia. (Fig. 1b).

In this study, we aimed to explore the climatic pattern over southern Tajikistan during the Early Pleistocene. For this purpose, we investigated the lower part of the Chashmanigar section through an excavation with a trench length of ~20 m and a trench depth of 1–7 m (Fig. 2). We present paleomagnetic research and the first rock magnetic study of the loess-paleosol sequence in the Chashmanigar section. Furthermore, we report the magnetic susceptibility and grain size records of the Chashmanigar section. The grain size and magnetic susceptibility records are compared with those of previous studies (Ding et al., 2002b) and the extension of the existing scheme scale for the loess deposits in southern Tajikistan is discussed.

2. Materials and methods

2.1. Sampling site and sample collection

The Chashmanigar loess section (38°23'25.87"N, 69°49'58.33"E) is located in southern Tajikistan about 16 km to the north of Khovaling region and 7 km to the south-west of Baldjuvon district, where loess deposits are widely distributed on river terraces and piedmonts. The climate in this region is characterized by warm, humid interglacial, and

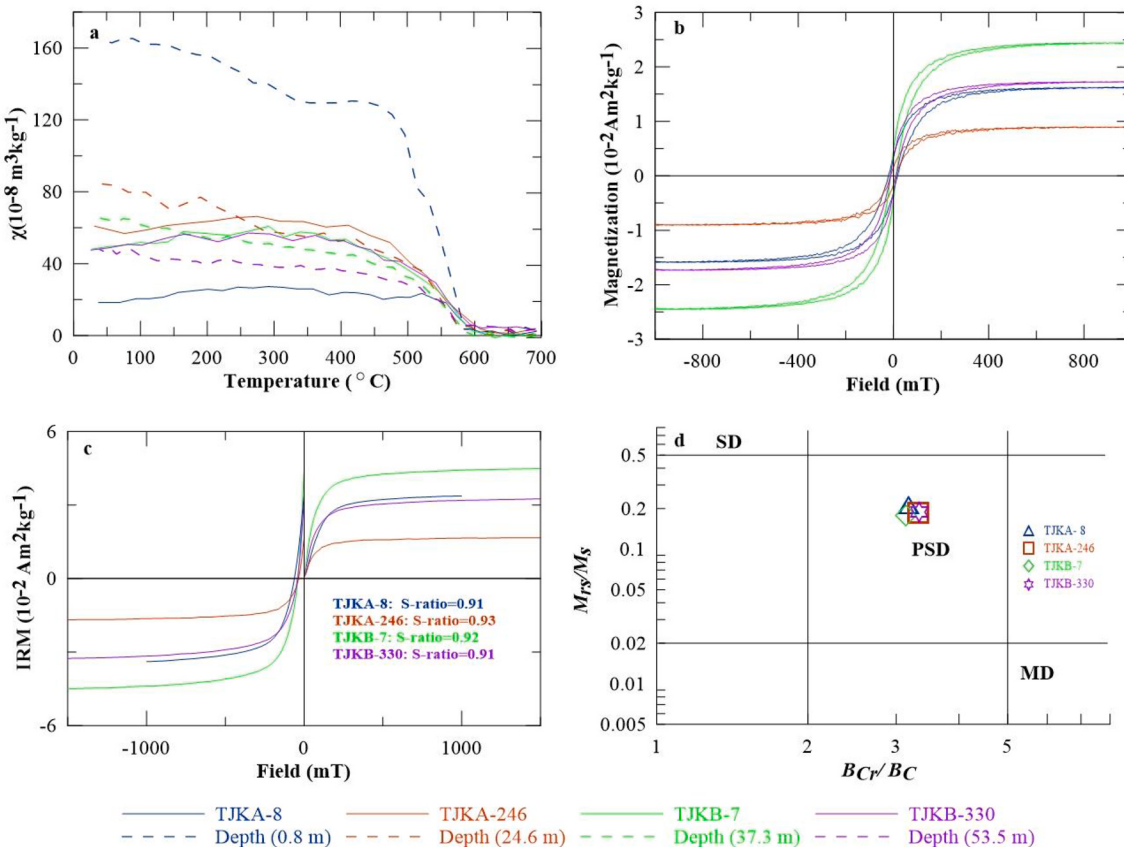


Fig. 3. Rock magnetic results of loess (TJKA-8, TJKB-7) and paleosol (TJKA-246, TJKB-330) samples from the Chashmanigar section. (a) Temperature-dependent magnetic susceptibility (χ -T) curves. Dotted (solid) lines indicate cooling (heating) curves. (b) Hysteresis loops after paramagnetic slope correction. (c) Acquisition of isothermal remanent magnetization (IRM) and back-field demagnetization of the saturation isothermal remanent magnetization (SIRM). SIRM is defined here as the IRM acquired in a magnetic field of 1.0 T. S-ratio = $0.5 \times [(-\text{IRM}_{-300\text{mT}}/\text{SIRM}) + 1]$ (Bloemendal et al., 1992). (d) 'Day plot' with SD (single domain), PSD (pseudo-single domain), and MD (multi-domain) zonations, after Dunlop (2002).

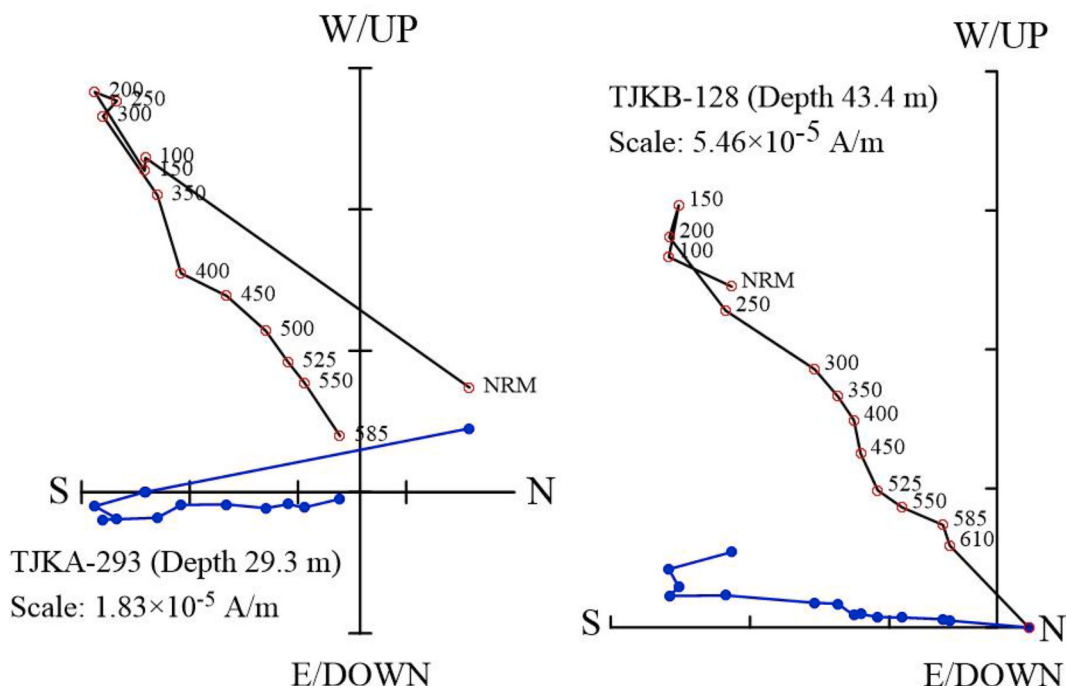


Fig. 4. Orthogonal projections of progressive thermal demagnetization of natural remanent magnetization (NRM) for two representative specimens from the Chashmanigar section. Solid (open) circles represent projections onto the horizontal (vertical) plane. Thermal demagnetization temperatures are indicated in °C.

dry, cold glacial. During the dry summer season, dust storms dominate the deserts and deflated aeolian dust is carried by westerly air streams to the east, where it rapidly settles down on entering the Pamir Plateau. During the wet winter season, dust storms basically disappear in the deserts with increased precipitation (Dodonov and Baiguzina, 1995). The rainy season begins in October and peaks during March and April before ending in May; little precipitation occurs between June and September (Häggi et al., 2019). At present, the mean annual temperature and precipitation at Chashmanigar are about 11–13 °C and 360–478 mm, respectively (Xian et al., 2015). During the summer months, dust transport and accumulation occur in Chashmanigar—storms from the Central Asian deserts transport dust to the piedmont of the Pamir mountains, where the rising air masses eventually lead to dust deposition (Dodonov, 1991).

The loess horizons in Chashmanigar section are characterized by yellowish, brownish color, massive structure, and some carbonate content (14–28%) (Dodonov, 1991). In the lower part of the section, the loess has low porosity. The paleosols are characterized by brownish or slightly reddish color and subangular blocky structure. The stratigraphic structure of the section can be roughly subdivided into two parts. The paleosols in the upper part of the section are much thicker and separated by thick loess layers, whereas they relatively thin and closely spaced in the lower part.

The whole Chashmanigar loess section is 220–227 m thick, and the lower part was blocked by slope wash. A 56-m section of the lower Chashmanigar with ~20 m of the lowermost trench was studied (Fig. 2), which allowed the acquisition of new results on the age and climatic patterns during the Early Pleistocene. From the Chashmanigar section, 763 samples were collected at 10 cm intervals from the top and at 5 cm intervals from the lowermost part of the section for grain size and magnetic susceptibility measurements. One hundred oriented block samples were collected at intervals of 20–30 cm for paleomagnetic analysis. The lowermost part of section (10–15 m) is unfortunately still covered by slumps.

2.2. Methods

All the pretreatments and measurements were performed at the Key Laboratory Institute of Geology and Geophysics, Chinese Academy of Sciences. The samples for grain size analyses were first treated with 10% H₂O₂ to remove organic matter and 10% HCl to remove carbonates. The sample residues were dispersed with 10 ml of 0.5 N (NaPO₃)₆ in an ultrasonic vibrator for 10 min and measured with the Malvern Mastersizer 3000 laser diffraction particle size analyzer. Low-frequency (0.47 kHz) magnetic susceptibility was measured using the Bartington MS3 magnetic susceptibility meter.

Oriented block samples for the paleomagnetic experiment were obtained at 20–30 cm intervals from the section. For further measurements, the block samples were dried and cut into 8 cm³ cube indoors. Before demagnetization, we performed systemic rock magnetic experiments (χ -T curves, hysteresis loop, isothermal remnant magnetization and back-field demagnetization characteristics) on selected samples. Progressive thermal demagnetization (14–17 steps) was performed on all the oriented specimens from room temperature to 610 °C, using the MMTD80 Thermal Demagnetizer. All remanences were measured using a 2G Enterprises Model 760-R cryogenic magnetometer installed in a magnetically shielded room (<300 nT).

Temperature-dependent susceptibility (χ -T curves) was measured using the MFK1-FA Kappabridge instrument equipped with a CS-4 high-temperature furnace, which can heat the samples from room temperature to 700 °C in an argon atmosphere to prevent oxidization. Hysteresis loops and isothermal remanent magnetization (IRM) acquisition curves and their backfield demagnetization characteristics were measured at room temperature using the MicroMag 3900 Vibrating Sample Magnetometer. The saturation magnetization, saturation remanence, coercivity and coercivity of remanence were calculated.

3. Results and discussion

3.1. Magnetic carrier mineral

The χ -T heating curves (Fig. 3a) display a slight increase in magnetic

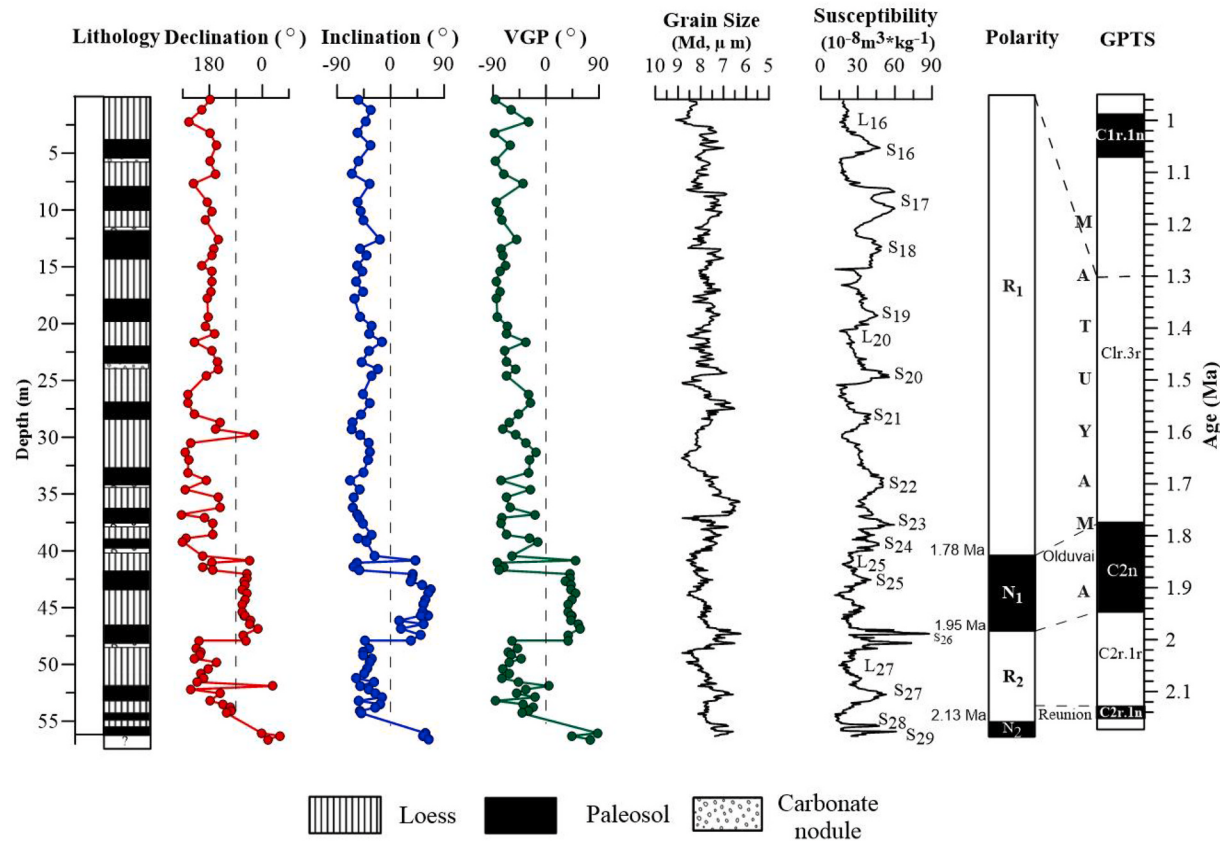


Fig. 5. Lithostratigraphy, particle size, magnetic susceptibility, and magnetic polarity stratigraphy for the Chashmanigar section, and correlation with the geomagnetic polarity time scale (GPTS) (Gradstein et al., 2012; Cohen and Gibbard, 2019).

susceptibility from room temperature to about 300 °C, probably due to the production of maghemite ($\gamma\text{Fe}_2\text{O}_3$) from some less magnetic Fe-hydroxides (Deng et al., 2005; Oches, 1996). All the heating curves for selected samples are characterized by a distinct decrease in magnetic susceptibility from 500 °C to 585 °C, and reach the minimum value at about 585 °C, i.e., the Curie point of magnetite (Fig. 3a), indicating the major contribution of magnetite to magnetic susceptibility. Due to the formation of weak maghemite resulting in a loss of magnetization during thermal treatment, the cooling curve is to some extent lower than the heating curve in some samples (Heller and Evans, 1995; Maher et al., 2010; Maher, 2011) (Fig. 3a). The main carriers of the magnetic signal minerals in loess and paleosol are magnetite. Based on the k-T curves and the hysteresis loop, the magnetic properties of the Chashmanigar section can be ascertained to be controlled by magnetite.

The hysteresis loops are almost closed completely in a field of 300 mT, indicating the dominance of low-coercivity ferromagnetic minerals (Fig. 3b). All the samples showed a rapid increase in IRM acquisition below 100 mT (Fig. 3c), and an acquired 91–97% of saturation isothermal remnant magnetization (SIRM) in a field of 300 mT. The back-field IRM demagnetization results show low coercivity of remanence (Bcr) values (<33 mT). These characteristics indicate that the predominant ferrimagnetic minerals are low-coercivity magnetic minerals. However, some IRM curves were still not completely saturated before 1 T and small gaps still existed in some hysteresis loops at 500 mT, indicating the presence of high-coercivity components. Combined with the behavior of thermal demagnetization, the highly coercive component is considered to be maghemite.

The S-ratio values of all the samples were close to 1 (Fig. 3c), showing the major contribution of low-coercivity magnetic minerals such as magnetite. Additionally, saturation magnetization (Ms), saturation remanence (Mrs), coercivity (Bc), and coercivity of remanence

(Bcr) values were determined and their ratios plotted on a “Day plot” of Mrs/Ms versus Bcr/Bc (Day et al., 1977; Dunlop, 2002) to determine the domain state of magnetite in the samples (Fig. 3d). All data were clustered closely within the pseudo-single domain (PSD) field, showing a similar grain size of magnetite throughout the loess sequence.

3.2. Magnetostatigraphy

Orthogonal projections of thermal demagnetization (Zijderveld, 1967) indicate that magnetization is dominated by a single or two components that can be resolved at demagnetization temperatures above a few hundred degrees Celsius (Fig. 4). Representative examples of thermal demagnetization diagrams for the Chashmanigar section are shown in Fig. 4 and the measured natural remanent magnetization (NRM) is characterized by two magnetic components. The first component was observed during initial demagnetization steps, until about <300 °C, and it was considered to probably represent a recent overprint with a viscous origin (Heller and Evans, 1995; Ding et al., 2002b). The second magnetization component was isolated in the temperature range from 300 °C or 400 °C–610 °C. A stable component was observed between 300 °C and 610 °C, and it is interpreted as a characteristic remanent magnetization (ChRM).

For calculation of ChRM directions, we performed principal component analysis (Kirschvink, 1980). A total of 100 (87%) samples with a maximum angular deviation of <15° yielded well-defined ChRM directions. Virtual geomagnetic pole latitudes from the ChRM vectors were used to develop the magnetic polarity stratigraphy (Fig. 5), and 4 magnetozones were identified in the studied section: 2 with normal polarity (N1–N2), and 2 with reversed polarity (R1–R2).

In the lower part of the Chashmanigar section, combined with the upper strata age constraints (Ding et al., 2002a, 2002b), the correlation

of studied polarity zones to the global geomagnetic polarity time scale (GPTS) (Gradstein et al., 2012) is straightforward. We correlated the top normal interval of N1 to subchron C2n, corresponding to a time interval of 1.78–1.95 Ma at a depth of 42–47 m. The top boundary of N2 at 56.2 m correlated to C2r.1r, the top boundary of Reunion (C2r.1n), was 2.13 Ma, providing an important age constraint for the magnetostratigraphy of the southern Tajikistan loess-paleosol sequences (Fig. 5).

3.3. Grain size and magnetic susceptibility

The grain size curve in Fig. 5 clearly expresses the loess-paleosol sequence. In the Chashmanigar section, loess horizons show coarser grain size values, while paleosols are characterized by fine grain size and median grain sizes in the ranges of 8.0–9.1 μm for loess units and 6.4–7.5 μm for paleosols. The median grain size of loess horizons is consistently coarser than that of paleosols, suggesting that during glacial periods, the intensity of the regional westerly winds was significantly enhanced or the deserts in Central Asia expanded, with respect to interglacial periods (Ding et al., 2002a, 2002b; Yang and Ding, 2008). The grain size curve shows no tracking changes between the line portion below and above the Olduvai, but coarsening of grain size occurred during the Reunion event.

The alternation of loess and paleosols is also clearly expressed in the magnetic susceptibility records (Fig. 5). Paleosols are characterized by consistently higher susceptibility values ($50\text{--}90 \times 10^{-8} \text{ m}^3/\text{kg}$) compared with the loess horizons ($<15\text{--}26 \times 10^{-8} \text{ m}^3/\text{kg}$) above and below them. Remarkably high susceptibility values could be often identified immediately below the paleosol horizons. A striking change of the susceptibility signature was observed near the Olduvai boundary (S_{26}) and around the Reunion boundary. The highest susceptibility values at Chashmanigar were measured in S_{18} , S_{26} , S_{28} , and S_{29} , whereas the susceptibilities of older complexes are generally low. The low-field magnetic susceptibility was considered to be a sensitive paleoclimate proxy for classic loess (Kukla et al., 1988). The phenomenon of magnetic susceptibility enhancement due to pedogenesis has been reported from loess-paleosols records in some Central Europe countries, such as the Czech Republic (Forster et al., 1996; Zhu et al., 2001), Poland (Nawrocki et al., 1996), Ukraine (Nawrocki et al., 1996; Tsatskin et al., 1998), and some Central Asian countries, such as Kazakhstan and Tajikistan (Ding et al., 2002b; Dodonov and Baiguzina, 1995; Forster and Heller, 1994), as well as loess deposits from the Midwestern United States (Geiss and Zanner, 2007). The glacial loess has lower susceptibility values, while the interglacial paleosol has higher susceptibility, which clearly suggests the formation of paleosols during past climate stages, when the climate was warmer and wetter than the colder and drier intervals.

3.4. Chronology and paleoclimatology of the tajik loess-paleosol sequences

For the Chashmanigar loess-paleosol sequences, all major geomagnetic polarity show reversals during ~ 1.3 and ~ 2.1 million years. In the Chashmanigar section, the exposed loess sequence above the slope wash was dated back to ~ 1.78 Ma (Ding et al., 2002b). In this study, we removed the slope wash part and the data provide a new concept of the age and paleoclimate of southern Tajikistan. The upper part of the profile studied by Ding et al. (2002b) corresponds to the Brunhes-Matuyama epoch. The lower part of the section (the dug trench) represents the Matuyama epoch to the Reunion subchron.

Measurements of rock magnetic studies show that magnetite with a PSD size is the dominant remanence carrier in the Chashmanigar loess-paleosol sequence. The lower part of the profile yields the long-reversed polarity (R1, R2), which could be attributed to the Matuyama epoch of reversed polarity. At this stage of the investigation, we place the Reunion boundary within L_{28} at a profile depth of 56.2 m. However, the underlying S_{29} complex remains enigmatic, inasmuch covered by slope wash. The loess-paleosol of the Chashmanigar section unambiguously

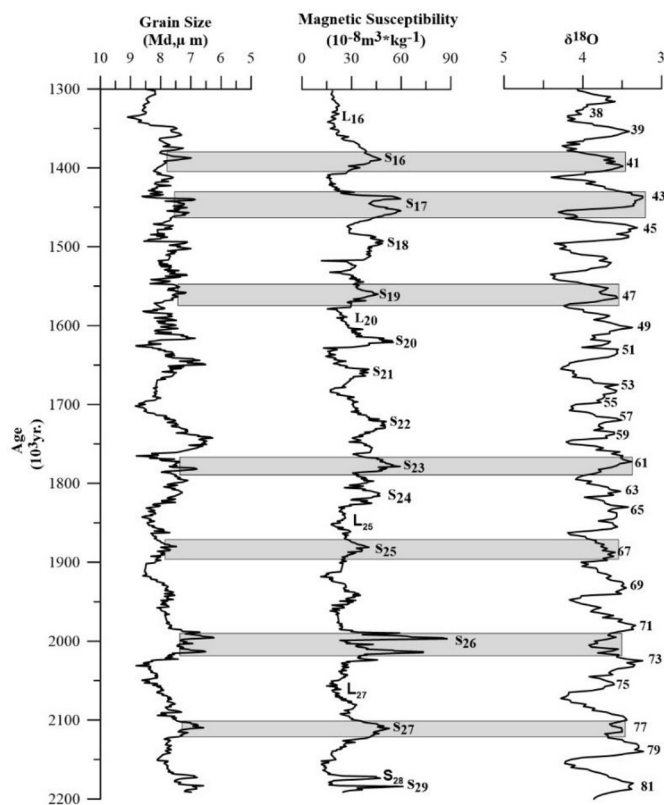


Fig. 6. Grain size, magnetic susceptibility, and deep-sea oxygen isotope records of the LR04 stack (Lisicki and Raymo, 2005) of the Chashmanigar section.

record all the main geomagnetic polarity reversals of the last 2.1 million years. Our results show that the formation boundaries are subchrons C2n–C2r.1n, suggesting an age range of 1.78–2.13 Ma for the lower Chashmanigar section.

Paleosols of S_{19} to S_{21} showed average magnetic susceptibility values around $\sim 40 \times 10^{-8} \text{ m}^3/\text{kg}$. S_{26} , S_{28} and S_{29} displayed higher susceptibility values (up to $\sim 90 \times 10^{-8} \text{ m}^3/\text{kg}$). Loess units, rich in carbonate, generally display very low magnetic susceptibility values ($\sim 15 \times 10^{-8} \text{ m}^3/\text{kg}$), partially attributable to the diamagnetism (weak, negative susceptibility) of carbonate minerals. The magnetic susceptibility values in paleosols are higher than those in loess units.

The median grain size of loess horizons is consistently coarser than that of paleosols, suggesting that during glacial periods, the intensity of the regional westerly winds was significantly enhanced or the deserts in Central Asia expanded, with respect to interglacial periods (Ding et al., 2002b). Apart from the wide variation in grain size between the loess and paleosols units, a second-order grain size change was also found within some loess or paleosol horizons such as S_{18} , S_{26} , L_{17} , and L_{22} (Fig. 5).

The loess-paleosol alternation, as well as its grain size and magnetic susceptibility changes, shows strong correlation with marine oxygen isotope records (Fig. 6). The loess intervals at Chashmanigar yielded low and fairly constant susceptibilities. Nevertheless, small-scale variations due to weak soil development even during cold climatic conditions were recorded in some loess layers. Visibly increased magnetic susceptibility in paleosols denote warmer and more humid climatic conditions. The trends of oxygen isotope records and continental records are remarkably similar during the Early Pleistocene, especially the last ~ 2.1 and ~ 1.3 Ma, and illustrate the global significance of the recorded paleoclimatic variations.

Table 1

Grain size and magnetic susceptibility results for the Chashmanigar section between ~2.1 and ~1.3 Ma based on a time scale.

Age (ka)	M.S. G. S.	G. S.																			
0	0	0	0	0	0	0	0	0	0	0	0	0	0	0	0	0	0	0	0	0	0
1270	18.4	8.5	1317	38.9	7.5	1344	23.4	8.0	1364	31.6	7.9	1418	41.6	7.8	1471	35.3	7.7	1501	26.9	7.9	
1271	18.2	8.2	1318	37.9	8.0	1345	25.8	8.2	1365	31.1	7.9	1419	37.4	7.7	1473	36.0	7.6	1502	26.6	8.1	
1272	17.6	8.2	1320	40.6	8.0	1345	30.6	8.3	1366	29.3	8.2	1421	11.7	7.7	1476	38.5	7.8	1502	26.6	8.0	
1273	18.8	8.2	1321	42.6	7.8	1346	36.8	7.9	1366	28.1	8.1	1422	26.8	8.1	1479	42.1	7.5	1502	28.4	7.6	
1275	19.4	8.3	1322	45.5	7.6	1346	54.9	8.1	1367	27.3	7.6	1423	28.0	8.0	1482	43.2	7.5	1502	27.4	7.5	
1276	18	8.4	1323	47.8	7.0	1346	79.2	8.6	1368	28.3	7.7	1424	28.3	8.0	1483	43.1	7.2	1503	28.0	7.8	
1277	19.9	8.5	1325	41.3	7.4	1347	81.6	8.5	1369	28.6	7.7	1425	30.2	8.1	1484	46.0	7.2	1503	28.1	8.0	
1279	20.3	8.4	1326	40.9	7.9	1347	59.7	8.1	1370	29.7	7.9	1426	29.7	7.8	1485	44.1	7.5	1503	30.5	7.7	
1280	21.8	8.4	1327	37.4	7.8	1348	49.3	7.0	1371	28.5	7.6	1428	32.7	8.0	1486	41.6	7.6	1504	36.7	7.4	
1281	22.5	8.5	1329	28.1	7.9	1348	47.3	6.9	1371	28.5	8.1	1429	31.8	7.7	1487	38.9	7.5	1504	30.1	7.7	
1282	20.5	8.6	1330	34.9	8.0	1349	42.8	6.9	1373	31.7	8.1	1430	31.9	8.0	1488	38.2	7.4	1504	30.2	8.2	
1284	21.3	8.5	1331	30.1	8.1	1349	42.3	7.9	1373	35.0	7.9	1431	30.8	7.7	1489	35.5	7.6	1505	32.7	8.2	
1285	21.1	8.6	1332	28.0	8.2	1350	41.4	7.4	1375	41.2	8.3	1432	29.5	7.7	1489	31.2	7.6	1505	30.3	8.1	
1286	22.3	8.6	1334	26.5	8.2	1350	40.6	7.4	1378	42.7	7.9	1433	29.5	7.7	1490	32.8	7.6	1505	35.4	7.7	
1288	22.3	8.5	1335	18.2	8.0	1351	41.9	7.2	1380	44.6	8.1	1435	26.7	7.9	1491	38.7	7.6	1506	32.3	8.2	
1289	19.4	8.5	1335	15.6	8.1	1351	43.0	7.2	1382	41.4	7.8	1436	24.3	7.4	1492	29.0	7.9	1506	34.5	7.7	
1290	17.7	8.7	1336	16.8	7.9	1352	44.2	7.3	1385	42.2	8.0	1437	16.9	7.8	1493	27.4	7.9	1506	36.2	7.2	
1291	20.4	9.1	1336	16.2	7.8	1352	47.3	7.6	1387	45.6	8.0	1438	22.8	7.5	1494	29.9	7.9	1507	32.8	7.3	
1293	18.1	8.8	1337	15.0	7.7	1353	51.7	7.4	1389	47.8	8.4	1439	24.5	7.5	1495	29.4	8.2	1507	43.9	7.1	
1294	15.5	8.6	1337	17.6	7.6	1353	50.7	7.1	1392	49.1	8.4	1440	27.9	7.7	1495	18.8	8.0	1508	49.5	7.2	
1295	19.4	8.7	1337	16.7	7.6	1354	55.4	7.6	1394	45.4	8.6	1441	30.5	7.2	1496	15.3	7.6	1509	46.7	6.9	
1297	19.4	8.4	1338	30.1	7.9	1354	58.7	7.4	1396	44.4	7.1	1442	31.1	7.1	1496	21.2	7.9	1510	48.2	7.1	
1298	20.1	8.3	1338	17.1	8.0	1355	59.8	7.4	1399	48.6	7.2	1443	29.9	7.8	1496	21.0	8.3	1511	54.7	8.0	
1299	17.1	7.6	1339	17.4	8.0	1355	57.1	7.8	1401	47.0	7.2	1444	32.7	7.4	1497	21.8	8.1	1512	48.6	8.2	
1300	21.9	7.5	1339	18.0	7.7	1356	57.0	7.5	1403	45.4	7.5	1445	28.9	7.7	1497	22.5	8.6	1514	55.2	8.4	
1302	22.4	7.7	1340	17.0	8.2	1356	55.4	7.1	1404	42.6	7.7	1446	35.1	7.9	1497	23.8	8.5	1515	40.4	8.3	
1303	20.8	7.6	1340	20.1	8.2	1357	53.3	7.1	1405	40.2	7.4	1447	32.4	8.3	1498	23.1	8.1	1516	40.9	8.4	
1304	21.1	7.4	1340	16.4	8.2	1357	49.5	7.3	1407	42.1	7.5	1448	33.6	8.1	1498	23.0	7.6	1517	40.7	8.0	
1306	28.2	7.3	1341	18.6	8.0	1358	49.1	7.2	1408	39.8	7.3	1449	37.3	7.7	1498	24.7	7.8	1518	38.5	8.4	
1307	23.9	7.5	1341	18.4	7.7	1358	46.6	7.5	1409	40.8	7.0	1450	33.3	7.8	1499	25.0	7.7	1519	34.5	8.8	
1308	25.3	8.0	1342	21.1	8.1	1359	44.4	7.6	1410	41.1	7.2	1451	31.9	8.1	1499	27.2	7.6	1520	29.4	8.8	
1309	31.3	8.1	1342	20.2	8.2	1359	42.3	7.6	1411	41.9	7.5	1454	31.1	8.4	1499	21.1	7.8	1521	12.9	8.3	
1311	33	7.9	1342	22.5	8.1	1360	41.8	7.7	1412	39.3	7.8	1457	34.5	7.6	1500	24.9	8.2	1522	18.6	8.3	
1312	34.7	7.8	1343	19.7	8.3	1361	40.3	7.7	1414	40.2	7.5	1459	33.4	7.5	1500	24.2	7.8	1523	21.2	8.0	
1313	34.5	7.7	1343	21.4	8.2	1362	37.9	7.7	1415	41.2	7.7	1462	32.5	7.5	1500	23.7	7.6	1524	18.7	8.1	
1315	36	7.9	1344	26.2	8.4	1362	34.6	7.7	1416	39.1	7.5	1465	33.6	7.4	1501	25.3	8.5	1525	15.6	7.8	
1316	38	7.3	1344	31.6	8.2	1363	34.3	7.8	1417	40.5	7.8	1468	33.3	7.4	1501	26.2	8.1	1526	16.9	7.9	
Age (ka)	M.S. G. S.	G. S.																			
1527	16.8	7.6	1572	19.1	8.2	1603	46.7	7.7	1704	33.4	7.5	1746	36.4	7.5	1772	18.4	8.5	1812	30.8	7.9	
1528	16.3	7.6	1573	17.2	8.2	1604	40.4	7.9	1705	31	8.3	1747	33.6	7.6	1772	17.6	8.4	1813	29.1	8.0	
1530	20.2	7.6	1574	17.6	8.2	1605	32.7	7.2	1707	33.7	8.1	1747	28.8	7.8	1773	18.6	8.4	1815	27.0	7.9	
1531	17.4	7.8	1575	17.1	8.2	1607	50.9	7.5	1709	34.4	8.1	1748	37.1	7.5	1774	19.7	8.4	1816	27.4	8.0	
1532	14.4	7.5	1575	17.5	8.1	1608	49.1	7.6	1711	36.7	8.8	1748	33.5	7.6	1774	20.6	8.2	1818	19.3	8.3	
1533	16.5	7.8	1576	20.9	8.2	1610	48.3	7.8	1713	39.4	8.4	1749	25.7	7.9	1775	24.9	8.3	1819	25.6	8.0	
1534	19.8	7.7	1577	22.6	8.2	1611	49.6	7.5	1714	46.2	8.1	1749	35.7	7.7	1775	21.7	8.2	1821	25.9	8.1	
1535	20.6	7.6	1578	21.1	8.1	1612	50.2	7.5	1716	45.4	8.4	1750	38.3	7.5	1776	23.7	8.1	1822	23.9	8.1	
1536	19.5	6.9	1578	24.9	8.2	1614	47.5	7.4	1717	48.8	7.5	1750	36.8	7.6	1776	28.3	7.9	1824	24.2	8.2	
1537	22.2	6.9	1579	27.9	8.2	1615	50.2	7.6	1719	48	8.0	1751	41.6	7.4	1777	28.7	7.9	1825	26.8	8.0	
1538	26.5	6.7	1580	31.5	8.3	1616	46.5	7.6	1720	47.3	8.0	1751	43.4	7.4	1777	29.4	8.2	1827	24.4	8.2	
1539	21.7	7.4	1581	27.8	8.1	1618	50.2	7.4	1722	50.3	7.4	1752	45.1	7.3	1778	27.9	7.9	1828	22.8	8.2	
1540	20.9	7.0	1581	27.5	8.0	1619	44.4	7.3	1723	50.7	7.4	1753	47.0	7.3	1778	24.6	7.7	1829	24.8	8.2	
1541	39.0	7.1	1582	29.1	8.1	1620	44.9	7.2	1725	52.8	7.5	1753	46.1	7.3	1779	24.8	8.3	1831	23.4	8.5	
1543	22.9	6.6	1583	30.9	8.2	1622	43.1	7.1	1726	55	7.5	1754	45.7	7.4	1779	28.0	8.3	1832	17.8	8.5	
1544	22.6	6.5	1584	30.6	8.2	1623	43.4	7.2	1728	54.1	7.6	1754	47.1	7.5	1780	25.9	8.3	1834	15.0	8.5	
1545	27.2	7.1	1584	33.7	8.5	1627	38	7.1	1729	59.4	7.5	1755	42.9	7.5	1781	26.9	8.3	1835	16.1	8.5	
1547	27.4	7.8	1585	31.1	8.5	1630	41.0	7.2	1731	46.3	7.7	1755	42.6	7.6	178						

Table 1 (continued)

Age (ka)	M.S. S.	G. S.																		
Age (ka)	M.S.	G.S.																		
1567	28.9	8.0	1596	38.4	8.2	1687	37.7	6.5	1743	39.4	7.4	1769	25.6	8.5	1805	36.5	7.8	1858	26.7	7.8
1568	29.3	7.8	1597	39.2	8.2	1690	41	7.1	1744	37.3	7.3	1770	24.2	8.4	1806	36.1	7.7	1860	25.1	7.8
1570	24.4	8.1	1599	39.3	7.8	1694	40.9	6.6	1745	43.3	7.1	1770	24.7	8.3	1808	36.2	7.7	1861	25.8	7.8
1571	26.4	8.2	1600	40.8	7.8	1698	42.4	6.7	1745	39.7	7.2	1771	21.4	8.4	1809	27.9	8.1	1863	25.6	7.8
1572	19.8	8.1	1601	40.3	7.9	1702	41.1	6.8	1746	39.4	7.3	1771	23.2	8.2	1811	32.4	8.0	1864	28.2	7.8
Age (ka)	M.S.	G.S.																		
1866	25.7	7.9	1931	48.6	6.95	1985	26.8	8.4	2035	30.6	7.8	2085	25.6	7.8	2045	28.7	8.1	2095	18.1	7.7
1867	31.8	7.7	1933	36.5	7.18	1987	22.3	8.3	2036	28.5	7.8	2086	26.7	7.7	2046	28.7	7.5	2096	17.6	7.7
1869	32.0	7.6	1934	55.2	6.91	1988	24.2	8.3	2037	25.7	7.7	2087	23.1	7.7	2047	29.0	7.6	2097	17.7	7.8
1870	34.4	7.6	1936	63.8	6.7	1989	23.3	8.3	2038	28.2	7.5	2088	24.3	7.7	2048	30.7	7.5	2098	20.5	7.9
1872	30.9	7.9	1937	66.6	6.62	1990	24.1	8.2	2040	28	7.4	2089	23.6	7.8	2049	30.0	7.6	2099	17.3	8.1
1873	35.3	7.6	1938	84.9	6.28	1991	27.3	8.1	2041	28.9	7.3	2090	20.9	7.7	2051	33.0	7.5	2100	11.7	8.1
1874	30.8	7.5	1940	87.8	6.24	1992	27.4	8.1	2042	23.2	8.0	2091	20.9	7.7	2052	36.1	7.5	2101	16.2	7.8
1876	32.0	7.9	1941	51.7	6.99	1993	25.3	8.2	2043	24.6	8.0	2093	18.2	7.8	2053	36.8	7.5	2102	16.0	7.8
1877	28.5	7.8	1943	23.0	7.29	1994	26.1	8.1	2044	26.2	7.8	2094	18.2	7.8	2054	39.1	7.3	2104	12.1	7.9
1879	26.6	7.8	1944	27.1	7.35	1995	24.4	8.2	2045	28.7	8.1	2095	18.1	7.7	2055	44.9	7.0	2105	11.7	7.9
1880	27.4	7.8	1946	26.0	7.29	1996	22.2	8.1	2046	28.7	7.5	2096	17.6	7.7	2056	45.8	7.0	2106	13.1	7.8
1882	32.5	7.6	1947	29.1	7.14	1998	17.7	8.6	2047	29	7.6	2097	17.7	7.8	2057	46.3	6.8	2107	14.2	7.8
1883	22.8	8.0	1949	26.8	7.24	1999	18.4	8.4	2048	30.7	7.5	2098	20.5	7.9	2058	49.4	6.8	2108	13.4	7.8
1885	30.8	7.8	1950	43.1	6.94	2000	18.8	8.4	2049	30	7.6	2099	17.3	8.1	2059	45.7	6.9	2109	14.8	7.8
1886	27.7	7.9	1951	33.6	7.38	2001	16.8	8.5	2051	33	7.5	2100	11.7	8.1	2061	47.6	6.8	2110	14.1	7.8
1888	28.5	8.0	1952	32.5	7.44	2002	20.3	8.1	2052	36.1	7.5	2101	16.2	7.8	2062	52.9	6.6	2111	14.0	7.8
1889	27.3	7.8	1953	33.8	7.46	2003	21.2	8.1	2053	36.8	7.5	2102	16.0	7.8	2063	50.3	7.0	2112	12.6	7.8
1890	18.1	8.0	1955	38.0	7.3	2004	14.9	8.3	2054	39.1	7.3	2104	12.1	7.9	2064	48.4	7.2	2114	13.7	7.7
1892	24.0	7.8	1956	40.0	7.24	2005	20.5	8.0	2055	44.9	7.0	2105	11.7	7.9	2065	46.0	7.3	2115	14.9	7.7
1893	25.2	7.8	1957	39.0	7.36	2006	21.4	8.1	2056	45.8	7.0	2106	13.1	7.8	2066	43.9	7.4	2116	15.3	7.8
1895	25.5	7.7	1958	54.8	7.1	2008	19.9	8.0	2057	46.3	6.8	2107	14.2	7.8	2067	43.2	7.4	2117	16.9	7.6
1896	18.4	8.1	1959	56.3	7.0	2009	23.4	8.0	2058	49.4	6.8	2019	20.3	7.8	2068	46.6	7.1	2118	15.9	7.6
1898	18.9	8.0	1960	73.4	6.6	2010	18.2	8.0	2059	45.7	6.9	2020	24.4	7.8	2069	43.3	7.2	2119	20.4	7.5
1899	22.6	8.0	1961	73.2	6.5	2011	18.5	7.9	2061	47.6	6.8	2021	22.9	7.7	2070	43.7	7.2	2120	24.4	7.1
1901	17.0	8.0	1962	55.6	7.0	2012	18.9	8.0	2062	52.9	6.6	2022	26.6	7.8	2072	42.0	7.3	2121	44.8	6.9
1902	20.5	8.0	1963	38.0	7.6	2013	20.5	8.1	2063	50.3	7	2023	23.8	7.6	2073	41.6	7.3	2122	44.8	6.9
1904	21.5	7.9	1964	39.2	7.5	2014	22.4	8.1	2064	48.4	7.2	2024	27.0	7.8	2074	40.2	7.4	2123	47.3	6.8
1905	22.3	7.8	1966	34.4	7.7	2015	20.4	8.0	2065	46	7.3	2025	29.9	7.8	2075	38.8	7.7	2125	39.0	7.2
1906	20.6	7.9	1967	35.4	7.8	2016	20.2	7.9	2066	43.9	7.4	2026	27.8	7.8	2076	33.4	7.8	2126	26.1	7.4
1908	21.6	7.7	1968	33.6	7.6	2017	22.7	8.0	2067	43.2	7.4	2027	30.2	7.6	2077	30.0	7.9	2127	19.0	7.5
1909	22.2	7.9	1969	34.5	7.8	2019	20.3	7.8	2068	46.6	7.1	2029	30.5	7.6	2078	24.7	7.7	2128	17.8	7.5
1911	21.3	7.8	1970	38.5	7.8	2020	24.4	7.8	2069	43.3	7.2	2030	33.0	7.5	2079	27.2	7.7	2129	16.2	7.5
1912	22.3	7.7	1971	45.7	7.4	2021	22.9	7.7	2070	43.7	7.2	2031	32.4	7.7	2080	32.1	7.7	2130	18.1	7.3
1914	24.2	7.8	1972	40.0	8.1	2022	26.6	7.8	2072	42.0	7.3	2032	32.0	7.7	2082	26.6	7.8	2131	18.0	7.4
1915	23.9	7.7	1973	27.1	8.3	2023	23.8	7.6	2073	41.6	7.3	2033	31.6	7.7	2083	25.9	7.8	2132	16.3	7.4
1917	22.7	7.7	1974	28.8	8.3	2024	27.0	7.8	2074	40.2	7.4	2034	31.1	7.8	2084	25.3	7.8	2133	22.9	7.2
1918	24.5	7.6	1975	24.1	8.5	2025	29.9	7.8	2075	38.8	7.7	2035	30.6	7.8	2085	25.6	7.8	2135	61.1	6.6
1920	24.5	7.7	1977	24.4	8.6	2026	27.8	7.8	2076	33.4	7.8	2036	28.5	7.8	2086	26.7	7.7	2137	33.4	6.8
1921	23.9	7.7	1978	27.7	8.4	2027	30.2	7.6	2077	30.0	7.9	2037	25.7	7.7	2087	23.1	7.7	2138	35.3	6.8
1922	22.6	7.7	1979	26.3	8.5	2029	30.5	7.6	2078	24.7	7.7	2038	28.2	7.5	2088	24.3	7.7	2139	36.4	6.8
1924	23.8	7.61	1980	19.3	8.8	2030	33.0	7.5	2079	27.2	7.7	2040	28.0	7.4	2089	23.6	7.8	2140	29.1	7.1
1925	30.6	7.32	1981	28.3	8.3	2031	32.4	7.7	2080	32.1	7.7	2041	28.9	7.3	2090	20.9	7.7	2141	26.0	7.2
1927	29.5	7.31	1982	25.1	8.4	2032	32.0	7.7	2082	26.6	7.8	2042	23.2	8.0	2091	20.9	7.7	2142	24.7	7.2
1928	33.6	7.26	1983	24.9	8.3	2033	31.6	7.7	2083	25.9	7.8	2043	24.6	8.0	2093	18.2	7.8	2143	30.0	7.4
1930	59.0	6.7	1984	24.0	8.4	2034	31.1	7.8	2084	25.3	7.8	2044	26.2	7.8	2094	18.2	7.8			

3.5. Paleoclimate significance of the tajik loess-paleosol sequences

3.5.1. Comparison with astronomically tuned oxygen isotope record

A Pliocene-Pleistocene stack of 57 globally distributed benthic $\delta^{18}\text{O}$ records was used for comparison, and correlations between climate records from North Atlantic sediments and Greenland ice were determined. In glaciations, when large volumes of isotopically light oxygen (^{16}O) are ‘locked up’ in continent-sized ice sheets, the proportion of isotopically heavy oxygen (^{18}O) in the oceans increases. The strong similarity between the Quaternary loess-paleosol grain size, magnetic susceptibility, and deep-sea oxygen isotope record (Fig. 6) provides compelling evidence of widespread stratigraphic integrity. During the interval 2.1–1.3 Ma, the composite $\delta^{18}\text{O}$ record can be divided into marine oxygen isotope stages (39–81) (Lisicki and Raymo, 2005). For this period, six large paleosol units (S₂₄–S₂₉) and six large loess units (L₂₄–L₂₉) were identified. The main peaks that indicate warm stages in the marine and land records were matched using the top and bottom of

these peaks as age control points.

The grain size composition of eolian deposits is determined by three factors: (1) characteristics of dust sources, (2) wind strength, and (3) sink-to-source distance (Pye, 1987). A grain size model was also employed to construct an independent chronology of Chinese loess (Porter and Zhisheng, 1995; Vandenberghe et al., 1997). Grain size records are in phase with the obliquity and precession curves, and exhibit similar amplitude modulation. The grain size of loess deposits is widely employed as a proxy indicator. The general trends in the LR04 stack and grain size and magnetic susceptibility records were strikingly similar for the 2.1–1.3 Ma period. The correlation between the Chashmanigar section and the composite $\delta^{18}\text{O}$ records (Fig. 6) show cycle by cycle correspondence between the records, and the records document a major shift in the dominant climatic periodicity from 41 ka to 100 ka (Ding et al., 2002b). This may have an important bearing on the forcing mechanisms for loess-paleosol alternations in southern Tajikistan, and the regional climate system controlling atmospheric dust deposition

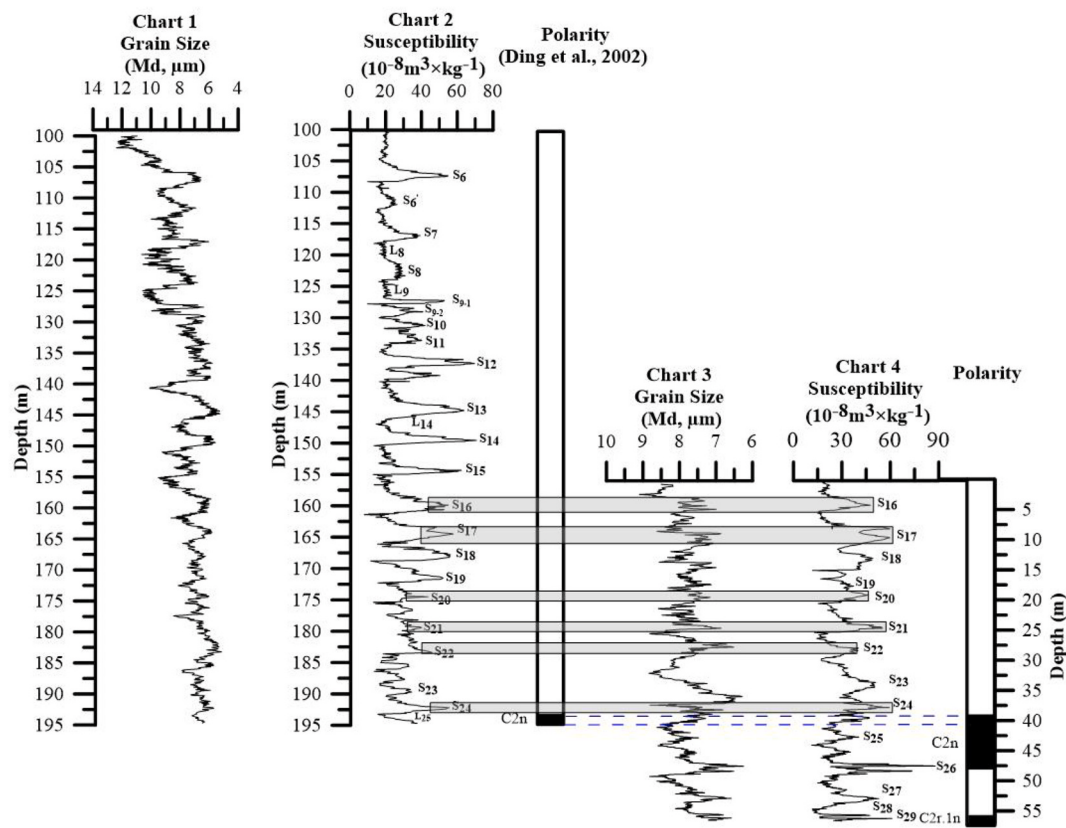


Fig. 7. Definition of grain size, magnetic susceptibility, polarity and crossing boundaries (Ding et al., 2002b), and new measurements. Chart-1 and Chart-2 illustrate grain size and magnetic susceptibility from the results of Ding et al. (2002b). Chart –3 and Chart-4 illustrate the results of new grain size, magnetic susceptibility, and polarity of the Chashmanigar section.

corresponds to global ice volume. On the global scale, the westerlies are links between the dust source (Asian arid inland) and deposition regions such as CLP (Sun et al., 2008a, 2008b; Zhang et al., 2014), North Pacific Ocean (Rea, 1994; Rea and Hovan, 1995), and polar ice (Xu et al., 2018) over the Northern Hemisphere. Westerly winds in the planetary circulation system in middle latitudes can be viewed as a link between the climates of the North Atlantic and Central Asian area. Cold-air activity in the high latitudes of the North Atlantic region has fundamentally influenced the Central Asian region through westerly winds and associated pressure systems. Successive studies of loess grain size composition have revealed “great prints” of North Atlantic cold events, in the last glaciation loess (Chen et al., 1997).

A recent study discovered that the humidity evolution exhibited a close link with the intensity of the westerlies in Central Asia (Jia et al., 2018). Moreover, the intensity of the westerlies is directly forced by the North Atlantic Oscillation rather than solar radiation during the Holocene (Jin et al., 2007). These cold-dry and dust-rich events are marked by visible loess sediments and by increases in the coarse fraction, suggesting strong instabilities in the westerlies-dominated climate during glacial times.

It is plausible that cold-air excursions of high-latitude, North Atlantic origin influenced the climate of Central Asia and also caused cold-dry events in the Asian monsoon areas. They might have been transmitted through the westerlies, suggesting that the westerlies may be a cold-air conveyor between the North Atlantic and the Global climate. Modeling studies have demonstrated that ice sheet growth and lower sea-surface temperature of the North Atlantic during the last glacial maximum led to an increase in the meridional (latitudinal) temperature gradient and southward migration of the polar front and the westerlies (Kutzbach et al., 1993). Therefore, the westerlies are most likely the link between

the climatic variations in the high north latitudes and Central Asia.

3.5.2. Lithological loess distribution in southern Tajikistan

Loess in southern Tajikistan (Tajik Depression) is comprised of deposited aeolian sediments interbedded with various paleosols, which have accumulated continuously over at least the last 2.1 Ma years. The tying depth to age clearly shows the loess-paleosol changes of the Chashmanigar section (Table 1). Loess accretion rates were high during glacial periods. During these eras, climatic conditions in Central Asia were cold and dry, resulting in more active dust sources and stronger northwesterly surface wind flows (Dodonov and Baiguzina, 1995; Kukla et al., 1988).

Overall, an additional ~20 m of the Chashmanigar loess-paleosol section was exposed in this study, relative to the previous study of this section by Ding et al. (2002b), by removing part of the slope wash, which provided the main age for loess deposits in southern Tajikistan (Figs. 6 and 7). Through the detailed stratigraphic investigation based on the new data of the Chashmanigar section, the main stratigraphic units of loess deposits widely distributed in southern Tajikistan could be identified (Fig. 8). These results provide important information for the concept of the stratigraphy of loess deposits in southern Tajikistan and Central Asia. The comprehensive loess sections are located in the basin of the Kyzylsu, Vakhsh, Obimazar, and Yaksu rivers (Fig. 1a). The Chashmanigar section (the biggest loess section) in southern Tajikistan has a subaerial formation in the watershed, ranging from 220 to 227 m. The subaerial strata represent a rhythmical sedimentation, revealed in sequences of loess and paleosols (Dodonov, 1991). Paleosols are clearly evident in sections of southern Tajikistan. Paleomagnetic data of the Chashmanigar section reveal the position of the Olduvai and Reunion boundary in the Early Pleistocene, which appears to be recorded by the

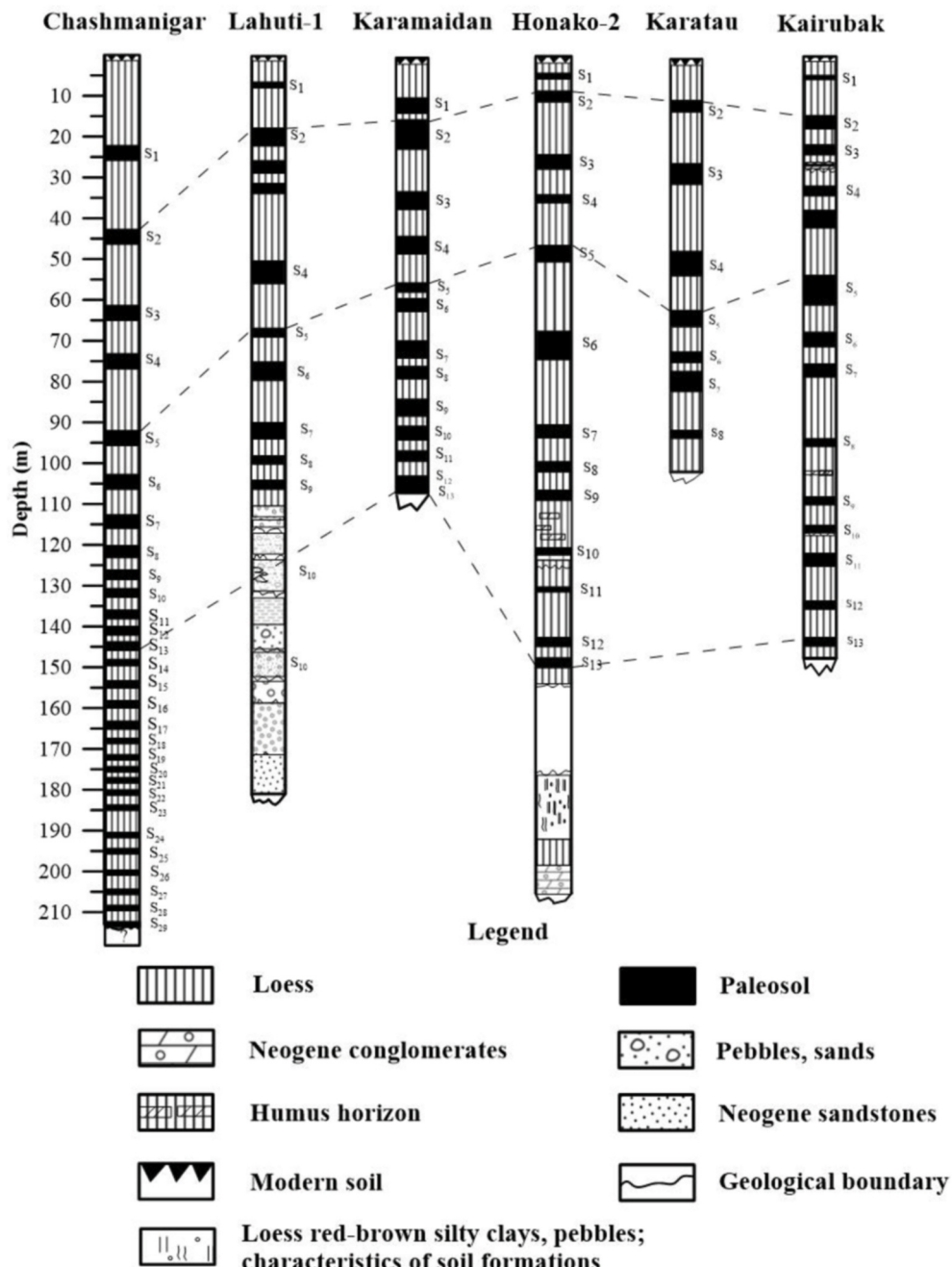


Fig. 8. Correlation scheme of loess-paleosol sections in southern Tajikistan. Modified after Dodonov et al., (1995).

S₂₄-S₂₉ paleosols. The thicknesses of the loess and paleosol horizons reach approximately 1–3 m and 3–7 m, respectively. Considering the conditions of geological occurrence, features of lithology, presence of ancient red-colored and red-brown paleosols, and paleomagnetic characteristics, it is reasonable to consider the subaerial deposits of older age generation as being correlated to alluvial-proluvial formations of the Kuruksay formation, whose age according to paleomagnetic data is defined as the Early Pleistocene. In general, the loess is observed to be wet and partially contain clay particles.

The Middle Pleistocene stages include loess and paleosols with predominantly brownish colors. The thicknesses of the loess horizons and paleosols reach 2–3 m and 5–7 m, respectively. These stages are characterized by pale yellow color, relatively unconsolidated grains, and porous structure, often manifested unevenly across the section. The paleosols in these complexes are characterized by relatively weak

leaching, significant vertical elongation of the profiles, and fuzziness of the illuvial carbonate horizons (Dodonov, 1991). The Upper Pleistocene stages consists of two superimposed or juxtaposed horizons between paleosol and loess with grayish-brown color. The paleosols in these complexes are characterized by relatively weak leaching, significant vertical elongation of the profiles, and fuzziness of the illuvial carbonate horizons. Fig. 8 illustrates the correlation between sections of southern Tajikistan. The loess-paleosol sequences (Lahuti-1, Honako-2 Karatau, Karamaidan, Kairubak) in southern Tajikistan are not as completable as the Chashmanigar section. The Chashmanigar section clearly demonstrates the global significance of the paleoclimate of Tajikistan and Central Asia, especially during the Early Pleistocene.

To some extent, the structure of the watershed loess-paleosol sequences of southern Tajikistan reflects the main geological boundaries coinciding with the boundaries of the Early Pleistocene, Middle

Pleistocene, and Upper Pleistocene.

4. Conclusions

Multiparameter rock magnetic investigations on loess deposits in the Chashmanigar section of Central Asia suggest that the predominant ferrimagnetic minerals in the study area are large PSD grains of magnetite, including limited maghemite.

We conducted paleomagnetic analysis and determined a new basal age of the Reunion subchron (2.13 Ma) for the Chashmanigar section, which provided clear information about the age of the loess deposits and a new extended stratigraphic scheme of southern Tajikistan. Using the stratigraphic scheme, the complete distribution of loess deposits in southern Tajikistan could be explained. The lower Pleistocene loess in the Chashmanigar section, with a basal age of ~2.1 Ma, is the oldest loess found so far in Central Asia.

Correlation of grain size and magnetic susceptibility with those by Ding et al., (2002aDing et al., 2002b 2002b) allowed the determination of the S₂₅–S₂₉ paleosols, which were blocked by slope wash. Through this correlation, the stratigraphy of the Chashmanigar section in southern Tajikistan could be clarified. However, the bottom of the section still remains blocked by slope wash.

The paleosols in the Chashmanigar section can be interpreted as having formed under relatively humid, calm, and warm climatic conditions with low atmospheric dust loadings. During the formation of the loess horizons, the climate in Central Asia was probably dry, windy, and cold with relatively high atmospheric dust loadings. The wind system transporting the Central Asian loess is closely related to the regional westerly winds during summer seasons.

The correlation of the Chashmanigar section with the oxygen isotope records from LR04 stack revealed the global significance of the recorded signals. Clearly, the fluctuation of grain size and magnetic susceptibility records suggest that the paleoclimate in southern Tajikistan (Central Asia) was controlled by the global climate on the orbital scale during the Quaternary period.

Declaration of competing interest

The authors declare that they have no known competing financial interests or personal relationships that could have appeared to influence the work reported in this paper.

Acknowledgments

This study was supported by the National Natural Science Foundation of China (Grant 41725010), Strategic Priority Research Program of the Chinese Academy of Sciences (GrantXDB26000000), Key Research Program of the Institute of Geology and Geophysics, CAS (GrantIGGCAS-201905), and “CAS-TWAS President Fellowship Program” of the Chinese Academy of Sciences (Grant). We also appreciate the comments and suggestions of reviewer and editor which have helped us to improve the manuscript.

Appendix A. Supplementary data

Supplementary data to this article can be found online at <https://doi.org/10.1016/j.quageo.2020.101114>.

Data availability

The data supporting the findings of this research can be found in Supplementary Data 1 or upon request from the author.

References

- Aizen, V.B., Aizen, E.M., Joswiak, D., Fujita, K., Takeuchi, N., Nikitin, S., 2006. Climatic and atmospheric circulation pattern variability from ice-core isotope/geochemistry records (Altai, Tien Shan and Tibet). *Ann. Glaciol.* 43, 49–60. <https://doi.org/10.3189/172756406781812078>.
- Bloemendal, J., King, J.W., Hall, F.R., Doh, S.J., 1992. Rock magnetism of late Neogene and Pleistocene deep-sea sediments: relationship to sediment source, diagenetic processes, and sediment lithology. *J. Geophys. Res.* 97, 4361–4375. <https://doi.org/10.1029/91JB03068>.
- Bronger, A., Winter, R., Heinkele, T., 1998. Pleistocene climatic history of East and Central Asia based on paleopedological indicators in loess-paleosol sequences. *Catena* 34, 1–17. [https://doi.org/10.1016/S0341-8162\(98\)00078-2](https://doi.org/10.1016/S0341-8162(98)00078-2).
- Chen, F.H., Bloemendal, J., Wang, J.M., Li, J.J., Oldfield, F., 1997. High-resolution multi-proxy climate records from Chinese Loess: evidence for rapid climatic changes over the last 75 kyr. *Palaeogeogr. Palaeoclimatol. Palaeoecol.* 130, 323–335. [https://doi.org/10.1016/S0031-0182\(96\)00149-6](https://doi.org/10.1016/S0031-0182(96)00149-6).
- Chen, F.H., Chen, J.H., Holmes, J., Boomer, I., Austin, P., Gates, J.B., Wang, N.L., Brooks, S.J., Zhang, J.W., 2010. Moisture changes over the last millennium in arid central Asia: a review, synthesis and comparison with monsoon region. *Quat. Sci. Rev.* 29, 1055–1068. <https://doi.org/10.1016/j.quascirev.2010.01.005>.
- Cohen, K.M., Gibbard, P.L., 2019. Global chronostratigraphical correlation table for the last 2.7 million years, version 2019 Q1-500. *Quat. Int.* 500, 20–31. <https://doi.org/10.1016/j.quaint.2019.03.009>.
- Day, R., Fuller, M., Schmidt, V.A., 1977. Hysteresis properties of titanomagnetites: grain-size and compositional dependence. *Phys. Earth Planet. In.* 13, 260–267. [https://doi.org/10.1016/0031-9201\(77\)90108-X](https://doi.org/10.1016/0031-9201(77)90108-X).
- Deng, C., Vidic, N.J., Verosub, K.L., Singer, M.J., Liu, Q., Shaw, J., Zhu, R., 2005. Mineral Magnetic Variation of the Jiaodao Chinese Loess//Paleosol Sequence and its Bearing on Long-Term Climatic Variability 110. <https://doi.org/10.1029/2004JB003451>.
- Ding, Z., Yu, Z.W., Rutter, N.W., Liu, T.S., 1994. Towards an orbital Ma or so over the Loess Plateau can be concluded, according time scale for Chinese loess deposits. *Quat. Sci. Rev.* 13, 39–70. [https://doi.org/10.1016/0277-3791\(94\)90124-4](https://doi.org/10.1016/0277-3791(94)90124-4).
- Ding, Z.L., Derbyshire, E., Yang, S.L., Yu, Z.W., Xiong, S.F., Liu, T.S., 2002a. Stacked 2.6-Ma grain size record from the Chinese loess based on five sections and correlation with the deep-sea δ₁₈O record. *Paleoceanography* 17, 1–5. <https://doi.org/10.1029/2001pa000725>, 5–21.
- Ding, Z.L., Ranov, V., Yang, S.L., Finaev, A., Han, J.M., Wang, G.A., 2002b. The loess record in southern Tajikistan and correlation with Chinese loess. *Earth Planet Sci. Lett.* 200, 387–400. [https://doi.org/10.1016/S0012-821X\(02\)00637-4](https://doi.org/10.1016/S0012-821X(02)00637-4).
- Dodonov, A.E., 1991. Loess of central asia. *Geojournal* 24, 185–194. <https://doi.org/10.1007/BF00186015>.
- Dodonov, A.E., Baiguzina, L.L., 1995. Loess stratigraphy of central asia: palaeoclimatic and palaeoenvironmental aspects. *Quat. Sci. Rev.* 14, 707–720. [https://doi.org/10.1016/0277-3791\(95\)00054-2](https://doi.org/10.1016/0277-3791(95)00054-2).
- Dunlop, D.J., 2002. Theory and application of the Day plot. *M. J. Geophys. Res.* 107, 1–22.
- Forster, T., Heller, F., 1994. Loess deposits from the Tajik depression (Central Asia): magnetic properties and paleoclimate. *Earth Planet Sci. Lett.* 128, 501–512. [https://doi.org/10.1016/0012-821X\(94\)90166-X](https://doi.org/10.1016/0012-821X(94)90166-X).
- Forster, T., Heller, F., Evans, M.E., Havlicek, P., 1996. Loess in the Czech Republic: magnetic properties and paleoclimate. *Studia Geophys. Geod.* 40, 243–261. <https://doi.org/10.1007/BF02300741>.
- Frechen, M., Dodonov, A., 1998a. Loess chronology of the middle and upper Pleis-tocene in Tadzhikistan. *Int. J. Earth Sci.* 87, 2–20.
- Geiss, C.E., Zanner, C.W., 2007. Sediment magnetic signature of climate in modern loess soils from the Great Plains. *Quat. Int.* 162–163, 97–110. <https://doi.org/10.1016/j.quaint.2006.10.035>.
- Gradstein, F.M., Ogg, J.G., Schmitz, M.D., Ogg, G.M., 2012. The geologic time scale 2012. <https://doi.org/10.1016/C2011-1-08249-8>.
- Häggi, C., Eglington, T.I., Zech, W., Sosin, P., Zech, R., 2019. A 250 ka leaf-wax δ_{13C} record from a loess section in Darai Kalon, Southern Tajikistan. *Quat. Sci. Rev.* 208, 118–128. <https://doi.org/10.1016/j.quascirev.2019.01.019>.
- Heller, F., Evans, M.E., 1995. Loess magnetism. *Rev. Geophys.* 33, 211–240. <https://doi.org/10.1029/95RG00579>.
- Jia, J., Lu, H., Wang, Y., Xia, D., 2018. Variations in the iron mineralogy of a loess section in Tajikistan during the mid-pleistocene and late pleistocene: implications for the climatic evolution in central asia. *G-cubed* 19, 1244–1258. <https://doi.org/10.1002/2017GC007371>.
- Jin, L., Chen, F., Ganopolski, A., Claussen, M., 2007. Response of East Asian climate to Dansgaard/Oeschger and Heinrich events in a coupled model of intermediate complexity. *J. Geophys. Res. Atmos.* 112, 1–14. <https://doi.org/10.1029/2006JD007316>.
- Kirschvink, J.L., 1980. The least-squares line and plane and the analysis of palaeomagnetic data. *Geophys. J. Roy. Astron. Soc.* 62, 699–718. <https://doi.org/10.1111/j.1365-246X.1980.tb02601.x>.
- Kutzbach, J.E., Guetter, P.J., Behling, P.J., Selin, R., 1993. Simulated climatic changes: results of the cohmap climate-model experiments. In: *Global Climates since the Last Glacial Maximum*. University of Minnesota Press, Minneapolis, pp. 24–93.
- Kukla, G., 1987. Loess stratigraphy in central China. *Quat. Sci. Rev.* 6, 191–219. [https://doi.org/10.1016/0277-3791\(87\)90004-7](https://doi.org/10.1016/0277-3791(87)90004-7).
- Kukla, G., Heller, F., Ming, LiuXiu, Chun, XuTong, Sheng, LiuTung, Sheng, AnZhi, 1988. Pleistocene climates in China dated by magnetic susceptibility. *Geology* 16, 811–814. [https://doi.org/10.1130/0091-7613\(1988\)016<811:PCICDB>2.3.CO;2](https://doi.org/10.1130/0091-7613(1988)016<811:PCICDB>2.3.CO;2) (1988).
- Liu, T.S., 1985. *Loess and the Environment*. China Ocean Press, Beijing, p. 251.

- Leroy, S.A.G., Kakroodi, A.A., Kroonenberg, S., Lahijani, H.K., Alimohammadian, H., Nigarov, A., 2013. Holocene vegetation history and sea level changes in the SE corner of the caspian sea: relevance to SW Asia climate. *Quat. Sci. Rev.* 70, 28–47. <https://doi.org/10.1016/j.quascirev.2013.03.004>.
- Lisiecki, L.E., Raymo, M.E., 2005. A Pliocene-Pleistocene stack of 57 globally distributed benthic δ 18O records. *Paleoceanography* 20, 1–17. <https://doi.org/10.1029/2004PA001071>.
- Maher, B.A., 2011. The magnetic properties of Quaternary aeolian dusts and sediments, and their palaeoclimatic significance. *Aeolian Res* 3, 87–144. <https://doi.org/10.1016/j.aeolia.2011.01.005>.
- Maher, B.A., Prospero, J.M., Mackie, D., Gaiero, D., Hesse, P.P., Balkanski, Y., 2010. Global connections between aeolian dust, climate and ocean biogeochemistry at the present day and at the last glacial maximum. *Earth Sci. Rev.* 99, 61–97. <https://doi.org/10.1016/j.earscirev.2009.12.001>.
- Nawrocki, J., Wójcik, A., Bogucki, A., 1996. The magnetic susceptibility record in the Polish and western Ukrainian loess-palaeosol sequences conditioned by palaeoclimate. *Boreas* 25, 161–169. <https://doi.org/10.1111/j.1502-3885.1996.tb00845.x>.
- Oches, E.A., Banerjee, S.K., 1996. Rock-magnetic proxies of climate change from loess-paleosol sediments of the Czech Republic. *Studia Geophys. Geod.* 40, 287–300. <https://doi.org/10.1007/BF02300744>.
- Pye, K., 1987. *Aeolian Dust and Dust Deposits*. Academic Press, London, p. 334.
- Porter, S.C., Zhiseng, A., 1995. Correlation between climate events in the North Atlantic and China during the last glaciation. *Nature*. <https://doi.org/10.1038/375305a0>.
- Rea, D.K., Hovan, S.A., 1995. Grain size distribution and depositional processes of the mineral component of abyssal sediments: lessons from the North Pacific. *Paleoceanography* 10, 251–258. <https://doi.org/10.1029/94PA03355>.
- Rea, D.K., 1994. The paleoclimatic record provided by aeolian deposition in the deep sea: the geologic history of wind. *Rev. Geophys.* 322, 159–195. <https://doi.org/10.1029/93RG03257>.
- Shackleton, N.J., Crowhurst, S.J., Weedon, G.P., Laskar, J., 1999. Astronomical calibration of oligocene-miocene time. *Philosophical Transactions of the Royal Society of London Series A-Mathematical Physical and Engineering Sciences* 357, 1907–1929. <https://doi.org/10.1098/rsta.1999.0407>.
- Sun, Y., Tada, R., Chen, J., Liu, Q., Toyoda, S., Tani, A., Ji, J., Isozaki, Y., 2008a. Tracing the provenance of fine-grained dust deposited on the central Chinese Loess Plateau. *Geophys. Res. Lett.* 35, 1–5. <https://doi.org/10.1029/2007GL031672>.
- Sun, D., Su, R., Bloemendal, J., Lu, H., 2008b. Grain-size and accumulation rate records from Late Cenozoic aeolian sequences in northern China: implications for variations in the East Asian winter monsoon and westerly atmospheric circulation. *Palaeogeogr. Palaeoclimatol. Palaeoecol.* 264, 39–53. <https://doi.org/10.1016/j.palaeo.2008.03.011>.
- Tsatskin, A., Heller, F., Hailwood, E.A., Gandler, T.S., Hus, J., Montgomery, P., Sartori, M., Virina, E.I., 1998. Pedosedimentary division, rock magnetism and chronology of the loess/palaeosol sequence at Roxolany (Ukraine). *Palaeogeogr. Palaeoclimatol. Palaeoecol.* 143, 111–133. [https://doi.org/10.1016/S0031-0182\(98\)00073-X](https://doi.org/10.1016/S0031-0182(98)00073-X).
- Van Den Berghe, J., Zhisheng, A., Nugteren, G., Huayu, L., Van Huissteden, K., 1997. New absolute time scale for the Quaternary climate in the Chinese loess region by grain-size analysis. *Geology* 25, 35–38. [https://doi.org/10.1130/0091-7613\(1997\)025<0035:NATSFT>2.3.CO;2](https://doi.org/10.1130/0091-7613(1997)025<0035:NATSFT>2.3.CO;2).
- Xu, B., Wang, L., Gu, Z., Hao, Q., Wang, H., Chu, G., Jiang, D., Liu, Q., Qin, X., 2018. Decoupling of climatic drying and asian dust export during the Holocene. *J. Geophys. Res. Atmos.* 123, 915–928. <https://doi.org/10.1002/2017JD027483>.
- Yang, S., Ding, Z., 2008. Advance-retreat history of the East-Asian summer monsoon rainfall belt over northern China during the last two glacial-interglacial cycles. *Earth Planet. Sci. Lett.* 274, 499–510. <https://doi.org/10.1016/j.epsl.2008.08.001>.
- Zijderveld, J.D.A., 1967. A.C. demagnetization of rocks: analysis of results. In: Collinson, D.W., Creer, K.M., Runcorn, S.K. (Eds.), *Methods in Paleomagnetism*. Elsevier, New York, pp. 254–286.
- Zhang, Y., Sun, D., Li, Z., Wang, F., Wang, X., Li, B., Guo, F., Wu, S., 2014. Cenozoic record of aeolian sediment accumulation and aridification from Lanzhou, China, driven by Tibetan Plateau uplift and global climate. *Global Planet. Change* 120, 1–15. <https://doi.org/10.1016/j.gloplacha.2014.05.009>.
- Zhu, R., Deng, C., Jackson, M.J., 2001. A magnetic investigation along a NW-SE transect of the Chinese loess plateau and its implications. *Phys. Chem. Earth, Part A Solid Earth Geod.* 26, 867–872. [https://doi.org/10.1016/S1464-1895\(01\)00134-X](https://doi.org/10.1016/S1464-1895(01)00134-X).